ARMY RESEARCH LABORATORY

Synthesis of Long-Chain-Branched (LCB) Polysulfones for Multifunctional Transport Membranes

by Andrew J. Duncan, Donald J. Leo, Timothy E. Long, and James F. Snyder

ARL-TR-5284 **September 2010**

NOTICES

Disclaimers

The findings in this report are not to be construed as an official Department of the Army position unless so designated by other authorized documents.

Citation of manufacturer's or trade names does not constitute an official endorsement or approval of the use thereof.

Destroy this report when it is no longer needed. Do not return it to the originator.

Army Research Laboratory
Aberdeen Proving Ground, MD 21005-5069

ARL-TR-5284 **September 2010**

Synthesis of Long-Chain-Branched (LCB) Polysulfones for Multifunctional Transport Membranes

Andrew J. Duncan, Donald J. Leo, and Timothy E. Long
Virginia Polytechnic Institute and State University

James F. Snyder
Weapons and Materials Research Directorate, ARL

REPORT DOCUMENTATION PAGE	Form Approved OMB No. 0704-0188

1. REPORT DATE *(DD-MM-YYYY)*	2. REPORT TYPE	3. DATES COVERED (From - To)
September 2010	Final	May 2007–September 2009

4. TITLE AND SUBTITLE
Synthesis of Long-Chain-Branched (LCB) Polysulfones for Multifunctional Transport Membranes

5a. CONTRACT NUMBER
ORISE-1120-1120-99

5b. GRANT NUMBER

5c. PROGRAM ELEMENT NUMBER

6. AUTHOR(S)
Andrew J. Duncan,* Donald J. Leo,* Timothy E. Long,* and James F. Snyder

5d. PROJECT NUMBER
DAAD19-02-1-0275 MAP MURI

5e. TASK NUMBER

5f. WORK UNIT NUMBER

7. PERFORMING ORGANIZATION NAME(S) AND ADDRESS(ES)
U.S. Army Research Laboratory
ATTN: RDRL-WMM-G
Aberdeen Proving Ground, MD 21005-5069

8. PERFORMING ORGANIZATION REPORT NUMBER
ARL-TR-5284

9. SPONSORING/MONITORING AGENCY NAME(S) AND ADDRESS(ES)

10. SPONSOR/MONITOR'S ACRONYM(S)
ARO MURI

11. SPONSOR/MONITOR'S REPORT NUMBER(S)

12. DISTRIBUTION/AVAILABILITY STATEMENT
Approved for public release; distribution is unlimited.

13. SUPPLEMENTARY NOTES
*The Macromolecules and Interfaces Institute, Virginia Polytechnic Institute and State University, Blacksburg, VA 24061

14. ABSTRACT
Long-chain-branched (LCB) polysulfones were synthesized for potential application as multifunctional ion-transport membranes. Combination of bulky and rigid monomer units with controlled levels of branching is proposed as a method to increase free volume of the polymer matrix. Increases in free volume may allow for improved ion transport decoupled from the segmental motion of the polymer backbone, especially in these high glass transition temperature materials. Increased transport in glassy materials enables multifunctional applications that require ion transport and structural rigidity. The series of novel polymers was characterized for chemical structure, thermal transitions, and molecular weight. Ionic conductivity was tested for films cast in the presence of two lithium salts.

15. SUBJECT TERMS
branched polymer electrolyte synthesis

16. SECURITY CLASSIFICATION OF:			17. LIMITATION OF ABSTRACT	18. NUMBER OF PAGES	19a. NAME OF RESPONSIBLE PERSON
a. REPORT	b. ABSTRACT	c. THIS PAGE			James F. Snyder
Unclassified	Unclassified	Unclassified	UU	22	19b. TELEPHONE NUMBER (*Include area code*) 410-306-0842

Standard Form 298 (Rev. 8/98)
Prescribed by ANSI Std. Z39.18

Contents

List of Figures **iv**

1. Introduction **1**

2. Experimental Materials and Methods **2**

3. Results and Discussion **4**

4. Summary **11**

5. References **12**

List of Symbols, Abbreviations, and Acronyms **14**

Distribution List **16**

List of Figures

Figure 1. $A_2 + B_2 + B_3$ synthesis of long-chain-branched PSF-PO. 5

Figure 2. (i) LIN-PSF-PO and (ii) LCB-0.4-PSF-PO analyzed with FTIR in (a) DMAc solution with (b) K_2CO_3 and (c) DHDPS for disappearance of the aromatic carbon-fluorine bond (664 cm^{-1}) from the monomers (d) BFP3O and (e) TFPPO reacting to form the polymers (f) LIN-PSF-PO and (g) LCB-0.4-PSF-PO (alphanumeric characters indicate each individual curve). 6

Figure 3. ^1H NMR spectra overlaid for the series of linear and branched PSF-PO. 7

Figure 4. SEC traces and molecular weight results for LIN-PSF-PO (maroon) and LCB-PSF-PO (mol % TFPPO: 0.2 = green, 0.4 = light blue, 0.6 = dark blue). 8

Figure 5. DSC heat capacity traces and T_g for LIN-PSF-PO (blue) and LCB-PSF-PO (mol % TFPPO: 0.2 = black, 0.4 = red, 0.6 = green). 9

Figure 6. DMA storage modulus and tan delta signals versus temperature showing T_g and sub-T_g transitions for LIN PSF-PO. 10

Figure 7. Combined Bode plot (|Z|, phase) for LIN-PSF-PO cast (blue: diamond, X) in the presence of Li^+ Tf^- (red: square, asterisk) or Li^+ Bim^- (green, up triangle, down triangle) against an empty background (black: circle, cross). 11

1. Introduction

Increasing numbers of technologies are based on the idea of harnessing charge transport for useful processes, such as energy harvesting, actuation, sensing, and permselectivity (*1*). Although much progress exists based on perfluorosulfonated platforms (Nafion,* $\sigma \approx 10^{-1} - 10^{-2}$ S/cm) new and more complicated parameters arise as applications require multifunctionality in engineering materials (*2*). For instance, in addition to using lightweight, durable, stable, high conductivity proton-exchange membranes in a fuel cell, it may be desirable to have the energy source bear load and operate as a structural installment. The most prevalent class of materials potentially capable of such a tradeoff are rubbery "salt-in-polymer" electrolytes that employ polymer segmental motion for transport of free ions from co-dissolved salts (*3*, *4*). Recently, Snyder et al. synthesized a series of "salt-in-polymer" electrolytes from various vinyl-ester resins, poly(ethylene glycol)s (PEO), and lithium trifluoromethanesulfonate (Li-Tf) (*5*). Various polymer topologies and other parameters were investigated, although none significantly varied the inverse relationship between mechanical stiffness and ionic conductivity. Another promising material class is conductive ionic glasses that demonstrate a high dielectric constant such that ion hopping through lattice defects provides sufficient conductivity in the glassy state (*6*). Imrie et al. did not investigate branching, but did show that liquid crystalline polyether sidegroups prevented packing of PEO sections of the main chain and resulted in increased conductivity in the glassy state (*7*). The multifunctional requirement starkly reflects the difficulty of using materials that display low ambient temperature modulus (especially when hydrated), including PEO and Nafion, or consideration of the significant decrease in ionic conductivity with the removal of the hydrating diluent/electrolyte. An overall approach to achieve both goals is to decouple ion transport from the segmental motion of the polymer through macromolecules designed to incorporate polar, bulky, irregular, rigid monomers into the backbone (*8*).

An $A_2 + B_2 + B_3$ polycondensation route is chosen to build upon existing methods and understanding of polymer branching (*9*). As reviewed, very few investigations exist concerning the effect of branching on decoupled ion transport in glassy, low humidity single-ion conductors. The chosen matrix of materials includes linear and long-chain-branched polysulfone phosphine oxides (LCB-PSF-PO). The use of polar B_2 and B_3 monomers will aid in the complexation of mobile ions from the imbibed salt within the matrix for charge stabilization and a decrease in the activation energy for ion hopping. The investigation of decoupled ion transport in such materials is also interesting for reasons of its implications in the electromechanical transducer field. Increases in ion transport without diluents or charges bound to the backbone are likely to augment ionic polymer transducer (IPT) performance through additive increases in ionic conductivity when introduced into ionomer composition and construction of the IPT composite.

*Nafion is a registered trademark of DuPont.

IPTs also do not require the same modulus levels as multifunctional batteries and fuel cells, thus providing a potential application for high conductivity composites that fall short of the structural target.

Previous systems demonstrated with PEO that three to four etheric oxygens serve to complex a single monovalent cation (*10*). Inclusion of branching into the system anticipates the difficult balance between establishing rigidity in the material while increasing intermolecular and intramolecular free volume for the purpose of complexation. To further extend the free volume effect, all chosen monomers are bulky in addition to their rigid nature, placing at least four aromatic rings in the backbone of each repeat unit. The monomers were recrystallized for purity before examining their characteristic spectra in comparison to the final polymers with Fourier transform infrared spectroscopy (FTIR). The final polymers are characterized with nuclear magnetic resonance (NMR) spectroscopy, size exclusion chromatography (SEC), thermogravimetric analysis (TGA), differential scanning calorimetry (DSC), and dynamic mechanical analysis (DMA). Films cast in the presence of Li-Tf and lithium bis(trifluoromethane)sulfonimide (Li-Bim) were also characterized for their ionic conductivity with electrical impedance spectroscopy (EIS).

2. Experimental Materials and Methods

4,4'-dihydroxydiphenylsulfone ([DHDPS], Alfa Aesar, 99.9%) was purified by dissolving in a 5% sodium bicarbonate solution and precipitation through adjustment of the pH to a value of 5 with concentrated hydrochloric acid. The crystals were redissolved in aqueous methanol (50%) for a final precipitation before drying *in vacuo* at 100 °C for 24 h (*11*). DHDPS was otherwise used as received from monomer grade material. Bis(4-fluorophenyl)phenylphosphine oxide ([BFP3O], Aldrich, 97%) was purified by recrystallization from toluene in triplicate. Anhydrous potassium carbonate (K_2CO_3) was purchased from Fluka and dried *in vacuo* at 120 °C for 24 h 1-bromo-4-fluorobenzene (99%). Magnesium, and phosphorous trichloride (99.9+ %) were purchased from Aldrich and used as received without further purification to synthesize the B_3 monomer, tris(4-fluorophenyl) phosphine oxide (TFPPO), according to previously reported procedures (*12*). Further supply of TFPPO was synthesized through oxidation of tris(4-fluorophenyl) phosphine (Aldrich, purum, 98.0% pure) with hydrogen peroxide (30 weight-percent). Dimethylacetamide ([DMAc], Aldrich, anhydrous, 99.8% pure) was stored over molecular sieves under a nitrogen atmosphere until use. Toluene (Aldrich, 98% pure) was dried using a fully contained solvent purification system and stored over molecular sieves under a nitrogen atmosphere until use.

DHDPS, BFP3O, TFPPO, K_2CO_3, DMAc, and toluene (2:1 v/v DMAc to toluene) were charged in a 100 ml three-neck, round-bottom flask at approximately 20 weight-percent solids in DMAc. The reaction setup was equipped with an overhead mechanical stirrer, a dry nitrogen inlet (with

condenser), and a Dean-Stark trap attached to a reflux condenser. The system was purged with nitrogen for 30 min before immersion in a constant temperature bath at 145 °C for 4 h, allowing reflux to remove the water/toluene azeotrope from the reaction mixture. Dropwise removal of residual water/toluene was performed during the temperature ramp to 165 °C. The reaction at 165 °C was allowed to proceed for approximately 110 h. The reaction solution was allowed to cool to ambient conditions without stirring while remaining under a nitrogen atmosphere. The reaction mixture was directly vacuum filtered with filter paper to remove the salt residue condensed by the reaction. The resulting polymer was precipitated into stirring deionized water. The polymers were collected by vacuum filtration and dried *in vacuo* at 250 °C for 1 h followed by a slow cooling under reduced pressure to room temperature. The polymers resulting from this synthesis are classified as linear (LIN) and long-chain-branched (LCB)-X where X is the mol percent of TFPPO incorporated into the polymer to enable branching.

The reaction solution and solutions of the final polymers were analyzed for disappearance of the aromatic carbon-fluorine bond on BFP3O and TFPPO with an ASI ReactIR 4000 *in-situ* FTIR Spectrometer. NMR analysis of the hydrogen (^{1}H) and carbon (^{13}C) nuclei in long-chain-branched polysulfones were performed using a Bruker 600 MHz spectrometer at ambient temperature in deuterated dimethylsulfoxide. Absolute molecular weights and polydispersity indices (PDI) were determined by SEC in a Waters system having three in-line Polymer Laboratories PLgel 5 μm MIXED-C columns with an autosampler. Detection is performed through a Waters 2414 Refractive Index detector, a Viscotek 270 Dual Detector viscometer, and a Wyatt Technologies miniDAWN multiangle laser light scattering (MALLS) detector in N-methyl pyrrolidone (NMP) at 50 °C. Thermogravimetric analysis was performed with a TA HighRes-2950 instrument at 10 °C/min under a nitrogen flow. Sub-ambient and high temperature thermal transitions were detected and analyzed with a TA Q1000 differential scanning calorimeter at 10 °C/min under a nitrogen flow. Transitions were determined from the second heat cycle. Membranes were cast from 10 weight-percent solutions in DMAc on level glass substrates. Casting was performed at approximately 40 °C under a heat lamp for 24 h. Sub-ambient and high temperature DMA was performed with a TA Q800 instrument at 10 °C/min under a nitrogen flow. Electrical properties of the polysulfone-phosphine oxide (PSF-PO) membranes were evaluated through EIS with an Autolab PGSTAT12 Potentiostat/Galvanostat and FRA2 Impedance Module over a frequency range of 1 MHz – 0.1 Hz. The instrument was operated in potentiostatic mode to apply a single 100 mV rms sine wave while measuring the complex impedance response of the sample. A custom fixture aligned two parallel rectangular brass rods at a defined separation of 0.3 cm to allow for in-plane impedance measurements with a maximum sample length of 3 cm. A load placed on top of the fixture ensured consistent and constant contact between the surface of the sample and the electrodes. All measurements were performed inside a custom-built Faraday cage and a humidity chamber at room temperature with controlled relative humidity of 42 ± 2%. Ionic conductivity values (σ, S/cm) were calculated with the equation:

$$\sigma = \frac{t}{R \cdot l \cdot w} \tag{1}$$

based on the in-plane two-point measurement geometry and an estimate of the bulk membrane resistance (R, Ohm) where t (cm) is the sample thickness, l (cm) is the sample length, and w (cm) is the sample width. The Autolab Frequency Response Analysis (FRA) software was employed to fit a circle to the kinetic portion of the complex impedance data (Nyquist plot) to extrapolate the bulk membrane resistance as the low frequency x-intercept where the imaginary component of the impedance equals zero. After mounting each sample, the impedance was measured to detect equilibration of the membrane with the chamber humidity. Measurements for calculation of the conductivity were not recorded until the change in impedance with time was less than 0.75% per minute. At this point, three to five impedance measurements were performed sequentially. The average value of the bulk impedance was used to calculate the membrane conductivity. One standard deviation typically represented no more than 10% error from the average value. Error was significantly smaller for less hygroscopic membranes.

3. Results and Discussion

Following their respective purification steps, the DHDPS (A_2), BFP3O (B_2), and TFPPO (B_3) were confirmed to be of suitable monomer grade purity for step-growth reactions by both thin layer chromatography and elemental analysis. The monomers were combined, as shown in figure 1, using 0, 0.2, 0.4, and 0.6 mol percent of TFPPO to facilitate the polymerization of long-chain branches from the backbone. Long reaction times were employed initially due to the expected decrease in reactivity of DHDPS compared to other bisphenols that have been demonstrated for polysulfones. Indicators for molecular weight development were mainly changes in viscosity of the reaction solution during the first screenings of the reaction.

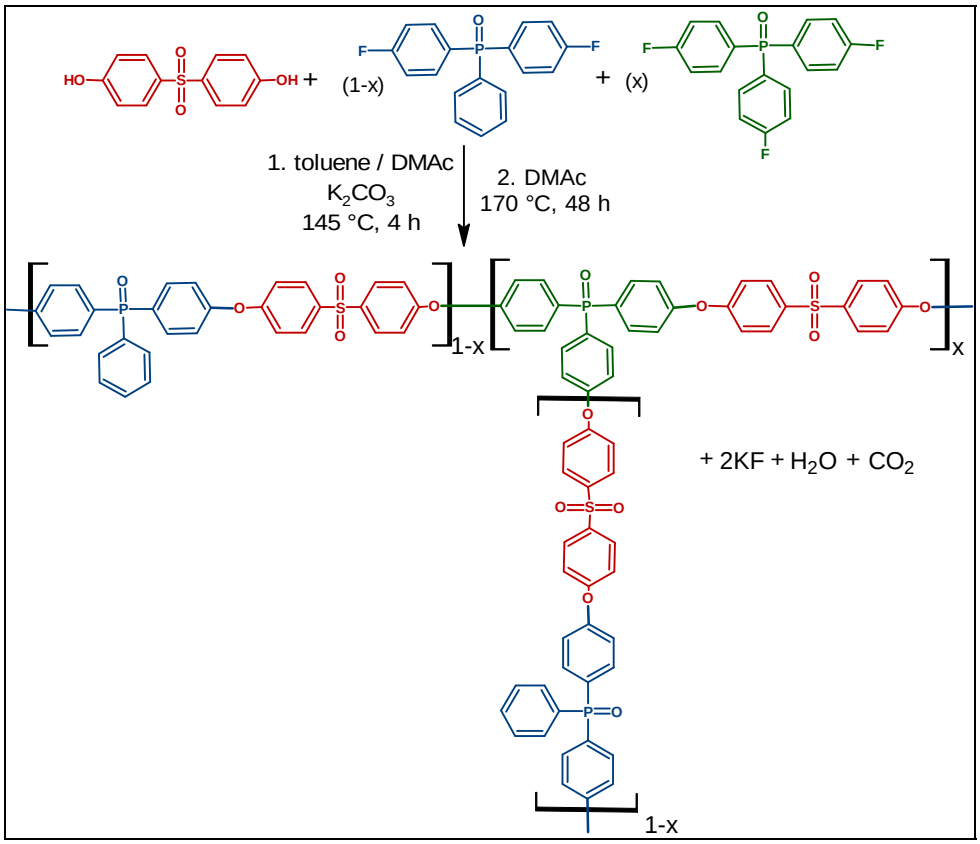

Figure 1. $A_2 + B_2 + B_3$ synthesis of long-chain-branched PSF-PO.

In-situ FTIR trials were planned to monitor molecular weight development in the backbone and branches due to condensation of the carbon-fluorine functionality on the aryl ring (carbon-fluorine bond at ~664 cm^{-1}) of BFP3O and TFPPO to the ester bond on reaction with DHDPS (*13*). Not only does this technique allow for estimation of sufficient time to reach near 100% conversion, but it also provides for observation of the limitations of converting the linear branch unit on the PSF-PO backbone to a dendritic one, namely the genus of a long-chain branch. However, the study only reached initial observations of the reaction solution, including all monomers, solvent, and reactants. Use of the FTIR also allowed for analysis solution spectra for linear polysulfone phosphine oxide (LIN-PSF-PO) and LCB 0.4 PSF-PO polymers, which are shown in figure 2 (i) and (ii) respectively. Comparison between those spectra of monomers and polymers in DMAc confirmed that the carbon-fluorine bond decreased significantly in the polymer and is a viable candidate to track with realtime *in-situ* FTIR.

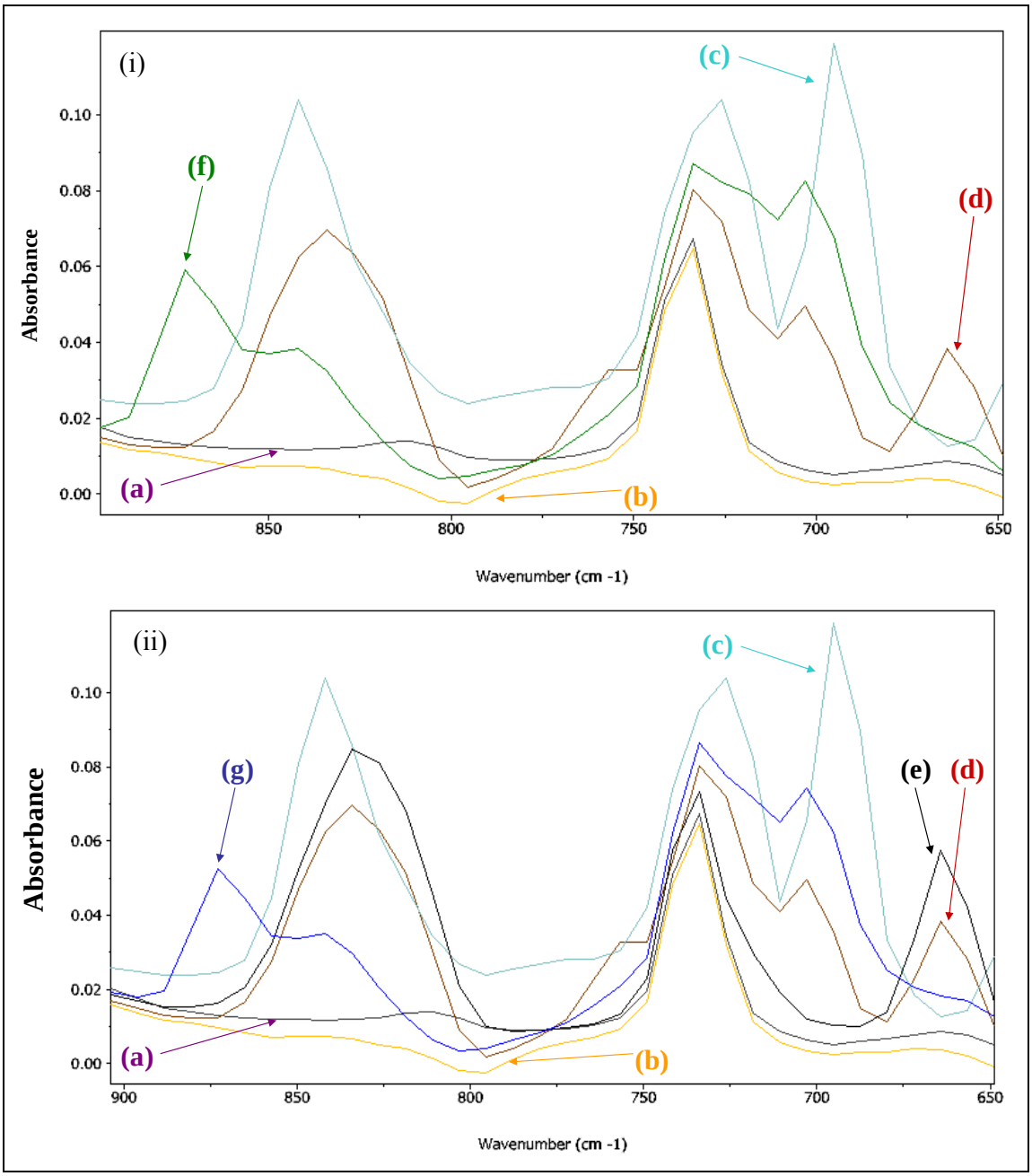

Figure 2. (i) LIN-PSF-PO and (ii) LCB-0.4-PSF-PO analyzed with FTIR in (a) DMAc solution with (b) K_2CO_3 and (c) DHDPS for disappearance of the aromatic carbon-fluorine bond (664 cm^{-1}) from the monomers (d) BFP3O and (e) TFPPO reacting to form the polymers (f) LIN-PSF-PO and (g) LCB-0.4-PSF-PO (alphanumeric characters indicate each individual curve).

The structure of the resulting long-chain-branched polymers (and linear analogue) was confirmed with shift assignment and integration of the corresponding peaks in ^{1}H NMR and ^{13}C NMR. A spectral comparison of the linear and branched polymers is provided in figure 3. The protons on the aromatic rings immediately adjacent to the sulfone display a shift at 8 ppm. Similarly located protons on the aromatic rings bonded to the phosphine oxide display a peak at

7.65 ppm. All aromatic protons adjacent to the etheric oxygen show a peak shift of 7.23 ppm. The small peak at 7.55 ppm is associated with the two opposing aromatic protons furthest from the backbone in BFP3O. Fluorine (^{19}F) NMR was planned to observe residual endgroups in the linear polymers, as well as the linear and terminal units from partially reacted TFPPO in the long-chain-branched polymers. The full distribution of branching efficiency, conversion to dendritic units, would also be visible in phosphorus (^{31}P) NMR with increasing inclusion of the B_3 unit and molecular weight. These characterizations were not available at the time of analysis and are yet to be completed.

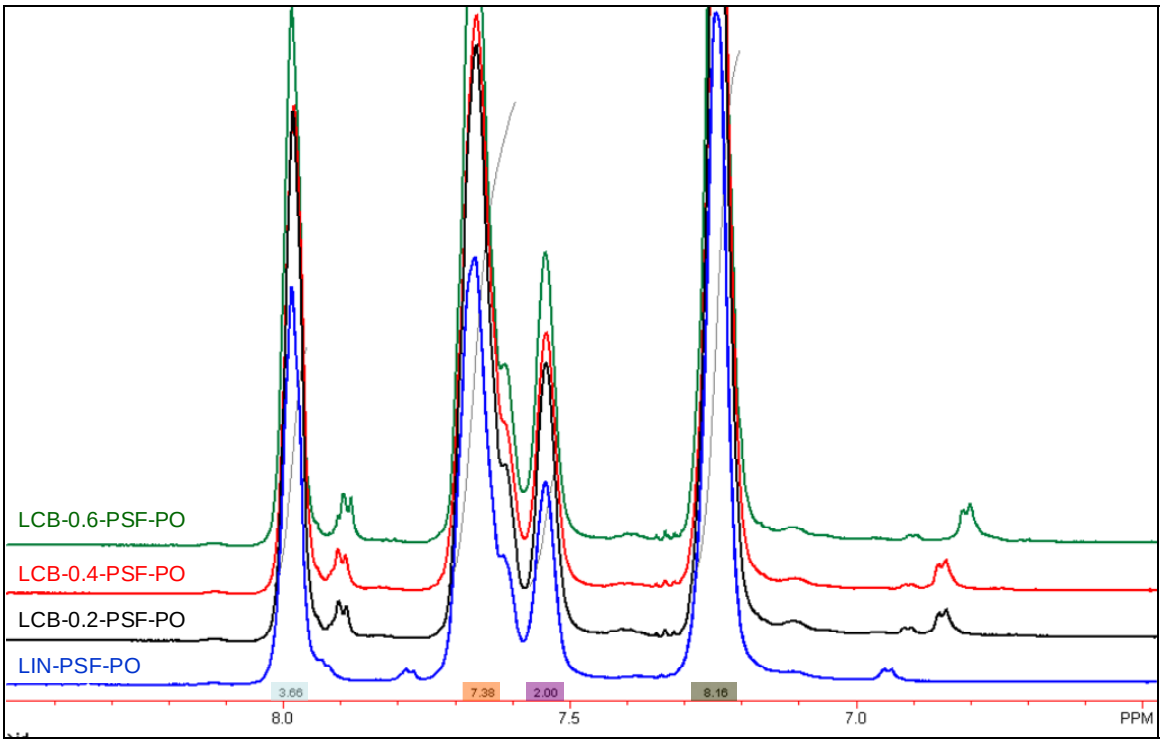

Figure 3. ^{1}H NMR spectra overlaid for the series of linear and branched PSF-PO.

Absolute molecular weights resulting from the $A_2 + B_2 + B_3$ reaction, as determined from the MALLS traces given by SEC analysis, are shown in figure 4. The curves are color coded to the molecular weight data. Curves not identified were other synthetic iterations that do not contribute to the discussion here. Development of molecular weight in the linear system is more easily achieved, almost by two times the molecular weight of the branched polysulfones. To qualify as long-chain branches, each branch must have an individual molecular weight greater than that of the entanglement molecular weight for the linear polymer. Although the degree of branching is not yet confirmed from NMR, the multi-modal peaks in SEC are typical of branched polymer elution. Due to the low level of total branching associated with long-chain branches, the polydispersity index is approximately equal to the linear sample and does not show the high values normally observed for hyperbranched systems (*14*). Overall, the final polymer molecular

weights from reactions with identical conditions may indicate that the development of molecular weight from the TFPPO (B_3) monomers is hindered as compared to reaction with the chemically similar BFP3O (B_2) monomer.

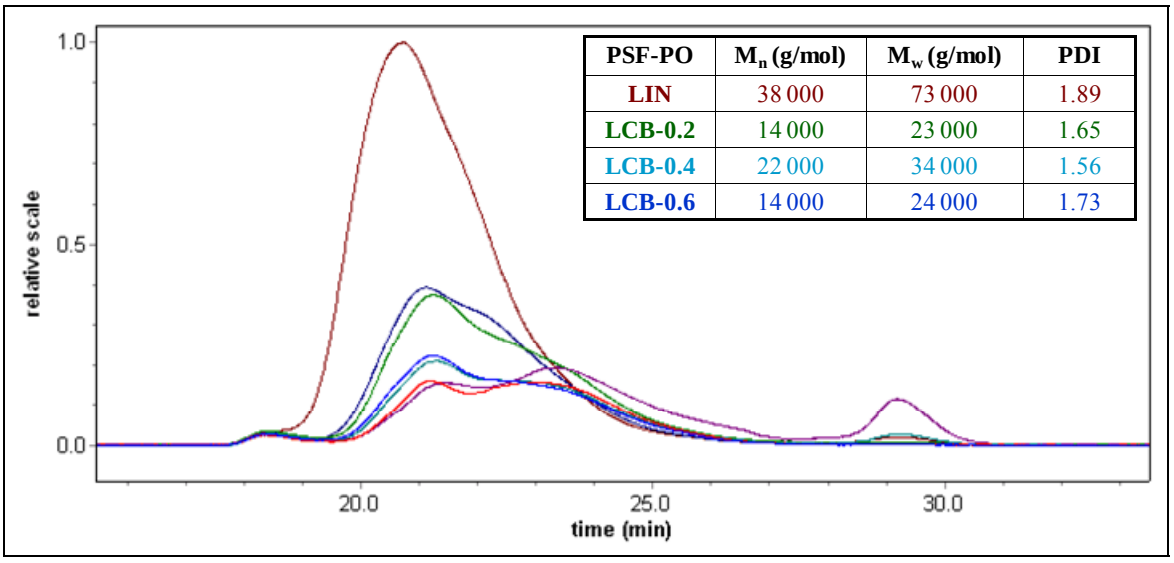

PSF-PO	M_n (g/mol)	M_w (g/mol)	PDI
LIN	38 000	73 000	1.89
LCB-0.2	14 000	23 000	1.65
LCB-0.4	22 000	34 000	1.56
LCB-0.6	14 000	24 000	1.73

Figure 4. SEC traces and molecular weight results for LIN-PSF-PO (maroon) and LCB-PSF-PO (mol % TFPPO: 0.2 = green, 0.4 = light blue, 0.6 = dark blue).

The thermal stability of the polymer series was investigated with TGA. Very little difference in degradation temperatures (5% weight loss, $T_{d5\%}$) is observed between the linear and branched samples or due to the level of branching. The average $T_{d5\%}$ is ~460 °C and proceeds quickly through two steps to a significant char yield (~20%) at 800 °C. The TGA test also reveals that even after drying these materials are very hygroscopic, likely due to the high concentration of polar groups in the backbone. The thermal transitions were initially observed with DSC. As expected, the effect of introducing low levels of long-chain branching has very little effect on the glass transition temperature (T_g) in comparison to the linear material. Based upon second heat measurements these fully amorphous polymers display a T_g between 231–236 °C for the linear and branched samples (figure 5). However, of greater interest is the comparison between the glass transition regions of the first and second heats. Although the speed of the cooling ramp associated with drying/annealing was not measured, the cool was not forced and is assumed to be much slower than the 10 °C cooling cycle programmed for DSC. Whereas the first heating cycle does not display any physical aging post-T_g, the second heat does display a maximum post-T_g, indicative of free volume isolated within the polymer during the cooling cycle (*15*). This characteristic is likely due to the use of rigid, bulky monomers that restrict the polymer from achieving its thermodynamic equilibrium during transition from the rubbery to the glassy state.

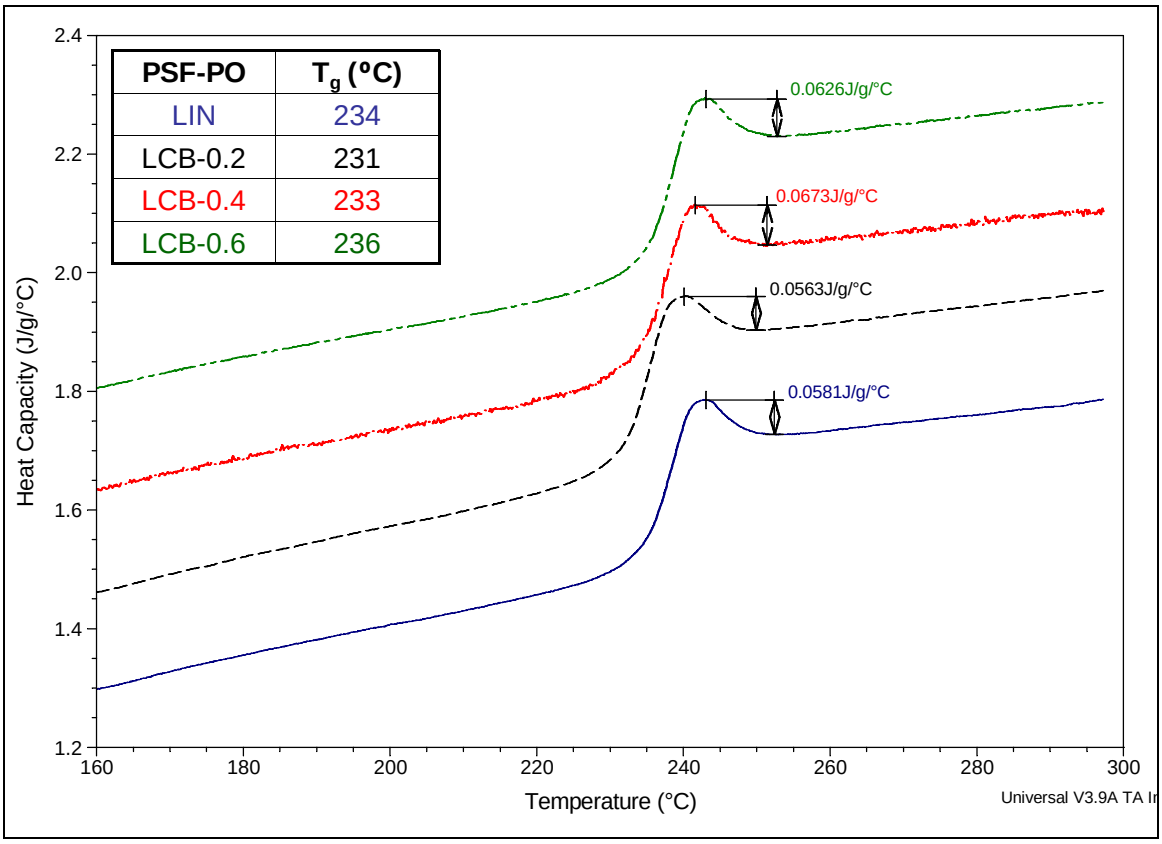

Figure 5. DSC heat capacity traces and T_g for LIN-PSF-PO (blue) and LCB-PSF-PO (mol % TFPPO: 0.2 = black, 0.4 = red, 0.6 = green).

The dynamic mechanical performance of these LIN-PSF-POs and LCB-PSF-POs was determined with DMA across a wide range of temperature (figure 6). It should be noted that casting films of the long-chain-branched polymers was severely limited, likely due to insufficient development of molecular weight. Tough films were characteristic for LIN-PSF-PO while the LCB series was very brittle. The linear film displayed a storage modulus of approximately 1 GPa in the glassy state across a wide range of temperature, which may be useful for structural applications. The appearance of the glass transition agrees with the range observed in DSC. Furthermore, at subambient temperature peaks are observed in the tan delta signal. The peak at 10 °C is likely the detection of free water melting in the hygroscopic polymer matrix. The lower beta transition at -100 °C is attributed to the aromatic rings of the backbone (and BFP3O sidegroup) flipping and twisting, which is typically observed in bisphenol-A polycarbonates or polysulfones of similar structure (*16*). These subambient motions are often attributed to toughening mechanisms in engineering thermoplastics.

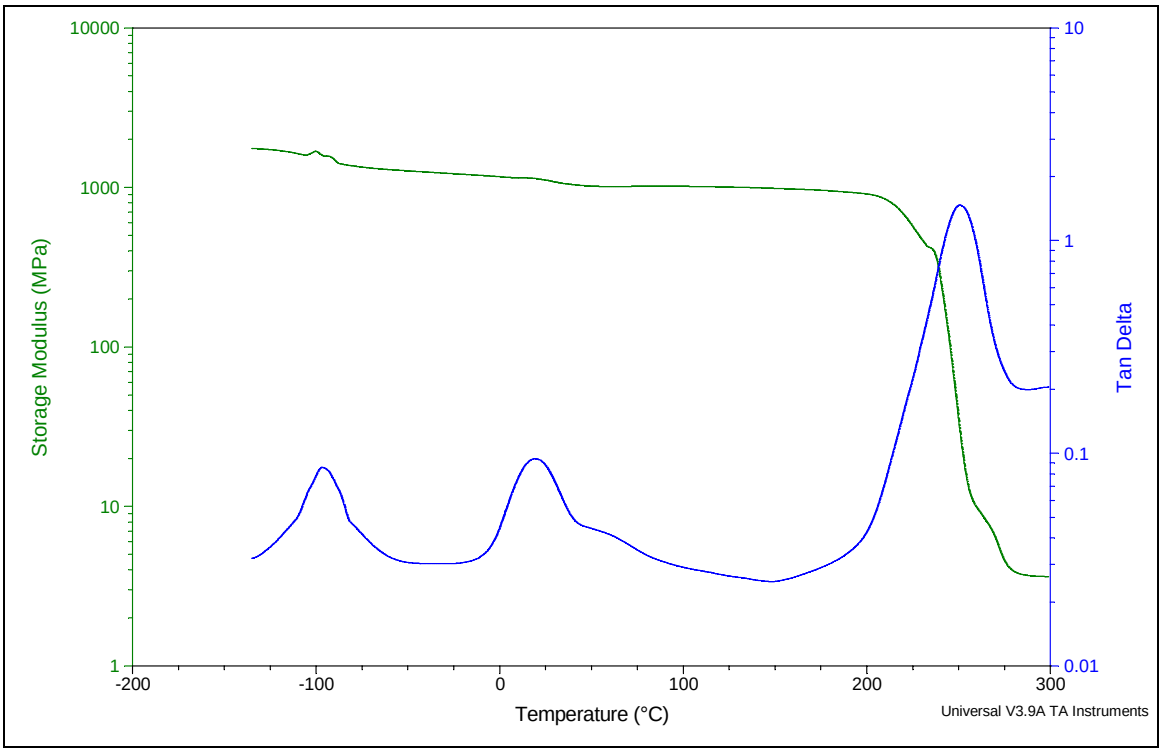

Figure 6. DMA storage modulus and tan delta signals versus temperature showing T_g and sub-T_g transitions for LIN PSF-PO.

As an initial test of the PSF-PO matrix as a host for conductive salts, membranes were cast from solution to contain 1:40 M:O of either Li^+ Tf^- or Li^+ Bim^-. A neat sample was also cast for comparison. In-plane electrical impedance measurements were carried out as shown in the Bode plot in figure 7. The impedance response of the membranes is also plotted against the baseline for the empty cell. The measurements were carried out at room temperature (22 °C) and a controlled relative humidity of 40% in a humidity chamber. Although there is some deviation from the baseline that begins around 10 Hz, all three membranes demonstrate the same trend. Although no direct estimate of the bulk resistance could be made based on the Nyquist plot, the value is likely to be above 10 GΩ. Also, it is possible that either changes in annealing of the membranes or changes in the salt ratio could further affect the resistance. Regardless, the PSF-PO matrix is has a very high resistance that may not allow for sufficient resolution of the effects of minor levels of branching.

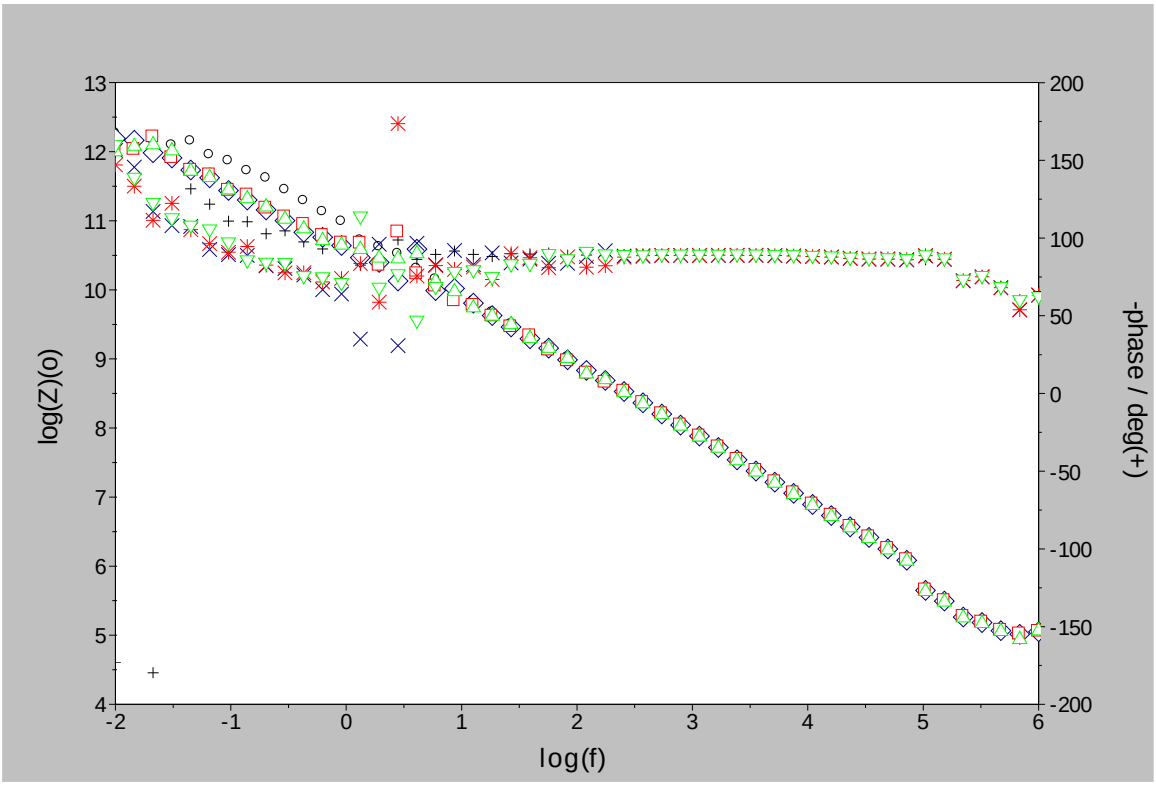

Figure 7. Combined Bode plot (|Z|, phase) for LIN-PSF-PO cast (blue: diamond, X) in the presence of Li^+ Tf^- (red: square, asterisk) or Li^+ Bim^- (green, up triangle, down triangle) against an empty background (black: circle, cross).

4. Summary

Linear and long-chain-branched poly(arylene ether sulfone phosphine oxide)s were synthesized by an A2 + B2 + B3 method without gelation. The structure and molecular weight were verified by NMR and SEC. The thermal transitions were observed through TGA, DSC, and DMA across a wide temperature range. Thermal analysis suggests that these polymers retain significant modulus while displaying higher than expected levels of hydrophilicity. The detection of physical aging due to enhanced bulkiness of the chosen monomers suggests an increase in free volume around the chain, which could be explored for complexation of ions during transport. However, the initial tests for membrane electrical properties demonstrated very high resistances potentially on the order of 10 GΩ, even when cast in the presence of conductive lithium salts. Further experiments are necessary to conclude if this result is due to overloading of the salt or truly the high bulk resistance of the membrane. Also, through-thickness measurements should be carried out to provide an estimate of charge transport in the primary direction of interest.

5. References

1. Kreuer, K. D. On the Development of Proton Conducting Materials for Technological Applications. *Solid State Ionics* **1997**, 1–15.
2. Mauritz, K. A.; Moore, R. B. State of Understanding of Nafion. *Chemical Reviews* **2004**, *104*, 4535–4585.
3. Mistry, M. K.; Subianto, S.; Choudhury, N. R.; Dutta, N. K. Interfacial Interactions in Aprotic Ionic Liquid Based Protonic Membrane and Its Correlation with High Temperature Conductivity and Thermal Properties. *Langmuir* **2009**, *25*, 9240–9251.
4. Angell, C. A.; Liu, C.; Sanchez, E. Rubbery Solid Electrolytes With Dominant Cationic Transport And High Ambient Conductivity. *Nature* **1993**, *362* 137–139.
5. Snyder, J. F.; Carter, R. H.; Wetzel, E. D. Electrochemical and Mechanical Behavior in Mechanically Robust Solid Polymer Electrolytes for Use in Multifunctional Structural Batteries. *Chemistry of Materials* **2007**, *19*, 3793–3801.
6. Forsyth, M.; Jiazeng, S.; MacFarlane, D. R. Novel High Salt Content Polymer Electrolytes Based On High Tg Polymers. *Electrochimica Acta* **2000**, *45*, 1249–1254.
7. Imrie, C. T.; Ingram, M. D. Decoupled ion Transport In Mesomorphic Polymer Electrolyte Glasses. *Electrochimica Acta* 2001, *46*, 1413–1417.
8. Wei, X.; Shriver, D. F. Highly Conductive Polymer Electrolytes Containing Rigid Polymers. *Chemistry of Materials* **1998**, *10*, 2307–2308.
9. McKee, M. G.; Unal, S.; Wilkes, G. L.; Long, T. E. Branched polyesters: recent advances in synthesis and performance *Progress in Polymer Science* **2005**, *30*, 507–539.
10. Berthier, C.; Gorecki, W.; Minier, M.; Armand, M. B.; Chabagno, J. M.; Rigaud, P. Microscopic Investigation of Ionic Conductivity in Alkali Metal Salts-Poly (Ethylene Oxide) Adducts. *Solid State Ionics* **1983**, *11*, 91–95.
11. Viswanathan, R.; Johnson, B. C.; McGrath, J. E. Synthesis, Kinetic Observations and Characteristics of Polyarylene Ether Sulphones Prepared Via a Potassium Carbonate DMAC Process. *Polymer* **1984**, *25*, 1827–1836.
12. Bernal, D. P.; Bedrossian, L.; Collins, K.; Fossum, E. Effect of Core Reactivity on the Molecular Weight, Polydispersity, and Degree of Branching of Hyperbranched Poly (Arylene Ether Phosphine Oxide)s. *Macromolecules* **2003**, *36*, 333–338.

13. Yilgor, I.; Mather, B. D.; Unal, S.; Yilgor, E.; Long, T. E. Preparation of Segmented, High Molecular Weight, Aliphatic Poly(Ether-Urea) Copolymers in Isopropanol. In-Situ FTIR Studies and Polymer Synthesis. *Polymer* **2004**, *45*, 5829–5836.

14. Czupik, M.; Fossum, E. Manipulation of the Molecular Weight and Branching Structure of Hyperbranched Poly(Arylene Ether Phosphine Oxide)s Prepared Via an $A_2 + B_3$ Approach. *Journal of Polymer Science, Part A: Polymer Chemistry* **2003**, *41*, 3871-3881.

15. Muggli, M. W.; Ward, T. C.; Tchatchoua, C.; Ji, Q.; Mcgrath, J. E. End-Group Effect on Physical Aging and Polymer Properties for Poly(Ether Sulfones). *Journal of Polymer Science, Part B: Polymer Physics* **2003**, *41*, 2850–2860.

16. Suga, T.; Wi, S.; Long, T. E. Synthesis of Diazocine-Containing Poly(Arylene Ether Sulfone)s for Tailored Mechanical and Electrochemical Performance *Macromolecules* **2009**, *42*, 1526–1532.

List of Symbols, Abbreviations, and Acronyms

^{1}H	hydrogen
^{13}C	carbon
^{19}F	fluorine
^{31}P	phosphorous
BFP3O	Bis(4-fluorophenyl)phenylphosphine oxide
DHDPS	4,4'-dihydroxydiphenylsulfone
DMA	dynamic mechanical analysis
DMAc	Dimethylacetamide
DSC	differential scanning calorimetry
EIS	electrical impedance spectroscopy
FRA	Frequency Response Analysis
FTIR	Fourier transform infrared spectroscopy
IPT	ionic polymer transducer
K_2CO_3	potassium carbonate
LCB-PSF-PO	long-chain branched polysulfone phosphine oxide
LCB-X	long-chain branched
Li-Bim	lithium bis(trifluoromethane)sulfonimide
Li-Tf	lithium trifluoromethanesulfonate
LIN	linear
LIN-PSF-PO	linear polysulfone phosphine oxide
MALLS	multiangle laser light scattering
NMP	N-methyl pyrrolidone
NMR	nuclear magnetic resonance
PDI	polydispersity indices

PEO	poly(ethylene glycol)
SEC	size exclusion chromatography
TFPPO	tris(4-fluorophenyl) phosphine oxide
TGA	thermogravimetric analysis

NO. OF
COPIES ORGANIZATION

1 (PDF only) DEFENSE TECHNICAL INFORMATION CTR
DTIC OCA
8725 JOHN J KINGMAN RD
STE 0944
FORT BELVOIR VA 22060-6218

1 DIRECTOR
US ARMY RESEARCH LAB
IMNE ALC HRR
2800 POWDER MILL RD
ADELPHI MD 20783-1197

1 DIRECTOR
US ARMY RESEARCH LAB
RDRL CIM L
2800 POWDER MILL RD
ADELPHI MD 20783-1197

1 DIRECTOR
US ARMY RESEARCH LAB
RDRL CIM P
2800 POWDER MILL RD
ADELPHI MD 20783-1197

1 DIRECTOR
US ARMY RESEARCH LAB
RDRL D
2800 POWDER MILL RD
ADELPHI MD 20783-1197

ABERDEEN PROVING GROUND

1 DIR USARL
RDRL CIM G (BLDG 4600)

2 US ARMY RESEARCH LAB
RDRL WMM G
J SNYDER
A DUNCAN